Stages of Flame Acceleration and Detonation Transition in a Thin Channel Filled with Stoichiometric Ethylene/Oxygen Mixture

Hung-Ping Chan[a] and Ming-Hsun Wu[a,b*]
[a] *Department of Mechanical Engineering, National Cheng Kung University, Tainan 70101, Taiwan*
[b] *Research Center for Energy Technology and Strategy, National Cheng Kung University, Tainan 70101, Taiwan*

1. Introduction

Flame propagation in small channels or tubes with cross-sectional dimensions approaching the characteristic lengths of reaction waves has recently drawn increasing research interests. Studies have been made on revealing the initial flame velocity growth, flame acceleration (FA), deflagration-to-detonation transition (DDT), and near limit detonation propagation characteristics in miniature confinements [1-9]. Better understandings of the phenomena are not only essential for the progress of fundamental combustion science, but also instrumental for the prevention of explosion hazards and the development of micro and meso-scale detonation engines [10]. Flame acceleration and DDT in narrow channels are relatively less understood although overall process of FA and DDT in large channels are well resolved in the early schlieren visualization by Oppenheim [11] and the extensive experimental, numerical and theoretical studies in the literature over the past 50 years [12-16]. The process typically started from the generation of laminar flame through a mild ignition source. The flame was stretched by the outward flow motion in the unburned gas region caused by the expansion of the burned gas in the confined channel. Volumetric burning rate increases with growing flame area, and flame instability is induced. Flame front becomes wrinkled under the influence of instability, and the propagation velocity is further enhanced with the inception of turbulence. Turbulent fluctuations can in turn excite more flame wrinkles. The positive feedback loop results in intense flame acceleration, which further leads to the formation of weak shocks at the flame front. Deflagration-to-detonation transition will then occur through interactions among shocks and the reaction front.

The flame propagation, acceleration and final transition to detonation may be quite different in miniature channels due to the enhanced heat loss and viscous friction. For example, turbulence in the induced flow ahead of the flame front is known to be instrumental for detonation initiation in macro scale channels, and this is why devices for tripping turbulence, such as Shelkin spirals, are widely installed in large detonation tubes to reduce DDT run-up distance and time. But flows are generally less turbulent in narrow channels in which Reynolds number is smaller due to the smaller characteristic length. If turbulence still plays the key role in flame acceleration and DDT in a small channel like its macro-scale counterparts, flame acceleration and DDT should become more difficult to occur in smaller channels, i.e.

Correspondence to: Ming-Hsun Wu minghwu@mail.ncku.edu.tw

longer run-up distance and time. Higher heat loss due to the larger surface-to-volume ratio in the smaller channels also hinder flame velocity growth. Experimental results [4-7] nonetheless show the opposite; detonation induction distance and time become smaller as the size of channel or tube is reduced. The numerous studies on FA and DDT in larger channels also indicate the importance of shock formation and their interactions with the reaction front for triggering detonation transition [11-16]. The enhanced viscous effect in the micro channels may expedite shock formations and lead to shorter DDT induction distance and time as observed in our previous chemiluminescence visualizations of reaction propagations in small tubes, channels, and gaps [4-7].

The objectives of the work are to experimentally reveal dynamics of shock and reaction fronts from ignition until transition to detonation. High-speed schlieren visualization technique was implemented to resolve the temporal evolutions of the fronts in a transparent narrow channel. Stages of FA and quasi-steady propagation of the fronts were identified using the velocity evolutions derived from the high-speed image sequences. Changes of shock and reaction front patterns accompanied with the transition of propagation phases were well-resolved in the study.

2. Experimental Setup

Cross-sectional area of the narrow channel studied in this work was 1 × 1 mm², and the overall length was 930 mm. The lateral dimension is approximately equivalent to 2 detonation cell size of the mixture. The channel was fabricated on a stainless-steel plate using laser cutting. Because schlieren imaging was going to be utilized, two transparent glasses were clamped onto the channel plate to enclose the channel. Holes were drilled at the ends of one of the glass window to allow the feeding and purging of gaseous mixtures. Electrodes were inserted at the center of channel through the windows. The final channel assembly with aluminum fixtures are shown in Fig 1.

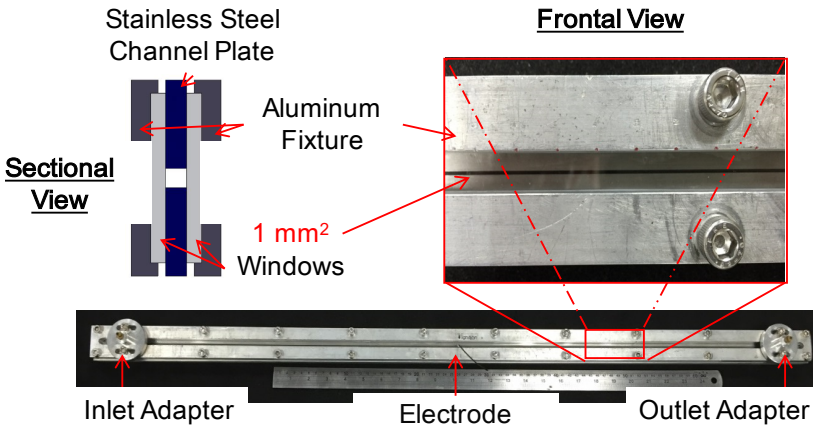

Figure 1. Narrow channel assembly for experiments. On the left side are shown the outer fixture frames to hole the glass plates onto the inner metal chamber plate.

To record the shock and reaction fronts evolutions, two high speed cameras are used (Phantom v12.1and MiroLab 310, Vision Research). Image sequences from the color camera (MiroLab 310) were used for checking the final reaction propagation mode, and the repeatability of the tests. The monochrome (Phantom v12.1) was used to capture the schlieren images of the reaction and pressure waves. A lens/mirror type schlieren system consisted of a 300 W xenon lamp source (Newport), a condenser lens, a

pinhole (diameter ~ 0.4 mm), a collimating lens and a de-collimating mirror was set up for the experiments. The plano-convex collimating lens with 20 cm focal length was 10 cm in diameter, and the focal length of the 8" mirror was 120 cm. With this set-up, the view region of the image was 4 cm in width. The schlieren images were recorded at a rate of 190,000 fps, and the exposure time was 0.285 μs.

Stoichiometric ethylene/oxygen mixture was fed into the channel through the inlet adapter at ambient temperature and pressure (298 K and 1 atm). The ethylene and oxygen flows were regulated by mass flow controllers (MKS Instruments). The flows were cut off and the filling-hose was unplugged from the adapter after 30 sec filling. The adapters on both sides were when the high-voltage circuit was triggered to generate a spark in the center of the channel for igniting the mixture. The voltage breakdown was recorded with a high-voltage probe, which was connected to a delayed signal generator that sent out signals to trigger the cameras. Details of the experimental set up can be found in Ref. [7].

3. Stages of Flame Propagations

Figure 2 shows the complete reaction front propagating scenario captured with the color high-speed camera. Only one side of the channel was shown in the figure since the evolutions were symmetric. After ignition, blue-colored deflagrative flame, which is relative dark comparing the detonative wave, starts to propagate and accelerate downstream. A very bright spot can be observed at the location where detonation transition occurs, and the detonation front propagates at nearly constant velocity thereafter. By measuring the distance traveled by the front between successive frames, we are able to derive the reaction front velocities. The reaction front velocity evolution obtained from the color high-speed chemiluminescence visualization is plotted in Figs. 3 along with the data extracted from schlieren visualizations. Since the view region was only 4 cm wide with current set up, the channel had to be shifted multiple times in the longitudinal direction to resolve the complete evolution along the channel. So, velocity data points from schlieren visualizations shown in Fig. 3 are actually a compilation of results from 15 separate tests under identical conditions. The scatter of the data points represents the uncertainty of the experiment. Also depicted in the figures are the velocity evolutions of leading and precursor shocks, which will be discussed later in section 4, resolved by the schlieren technique.

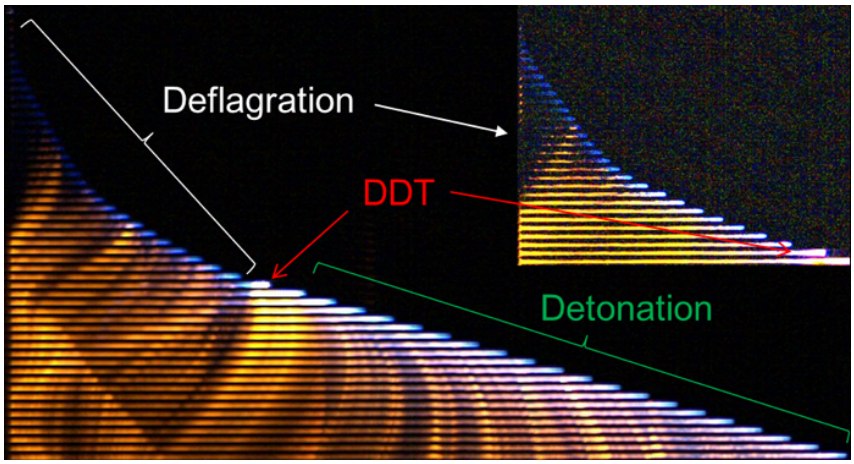

Figure 2. Chemiluminescence image of deflagration to detonation transition process.

By collating reaction and shock fronts velocities derived from the high-speed visualizations, 4 reaction propagation stages can be identified prior to the final transition to detonation. The four stages are named

as 1st FA, quasi-steady, 2nd FA and 3rd FA stages as shown in Figs. 3(a). The initial velocity of the reaction wave measured with the high-speed image sequences is around 80 m/s, which is comparable to the product of laminar flame speed and expansion ratio of stoichiometric ethylene/oxygen flame. The reaction front quickly accelerates to ~ 380 m/s within 30 μs and then travels at nearly constant velocity for another 25-30 μs. Two more acceleration phases are distinguished after the quasi-steady propagation and before the velocity surge associated with detonation transition. It is worth to note that the scatter of data points near the end of the 3rd FA stage in V-t (Fig. 3(a)) and V-x (Fig. 3(b)) charts is due to the larger experimental uncertainties among the test runs because of the higher propagation velocities in this phase. The velocity growth of the 2nd FA stage can be fitted using a power law curve, while the acceleration of the 3rd FA phase is linear. Besides, velocities of the fronts cannot be obtained from schlieren visualizations after detonation transition because the distance that the detonation wave travels between successive high-speed frames exceeds the width of view region.

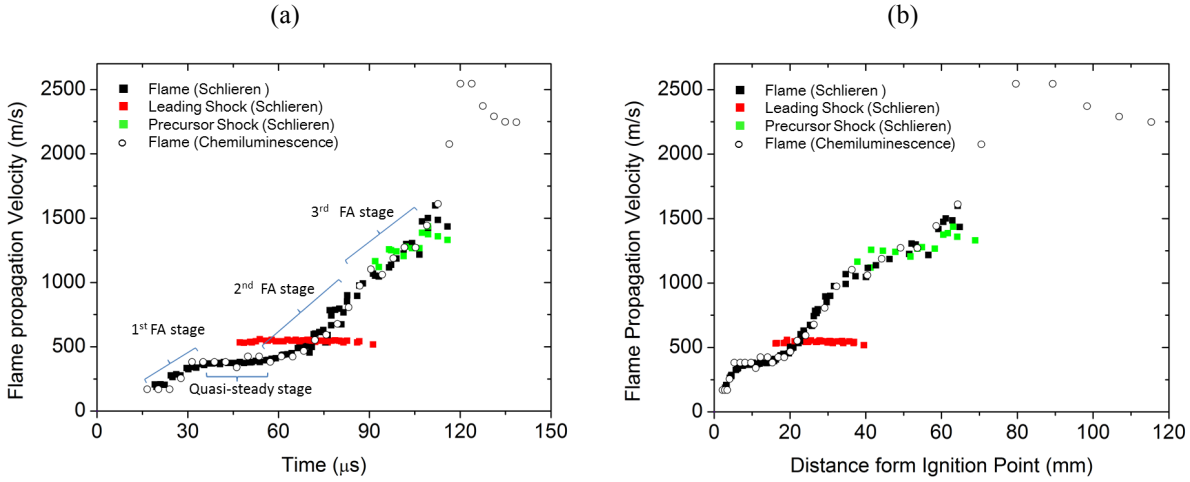

Figure 3. (a) V-t and (b) V-x plot derived from both, chemiluminescence and schlieren visualizations.

4 Dynamics of Reaction and Shock Fronts

Progressions of the reaction and shock fronts resolved by the schlieren visualization in the 1st FA, quasi-steady and 2nd FA stages are shown in Fig 4. There is a small invisible region at the left end of each picture due to obstruction by the ignition spark electrodes. A smooth parabolic flame front emerged from the blocked igniter region at 17.07 μs after voltage breakdown in the figure. The flame then propagates towards the right with a mild acceleration. Expansion of burned gas behind the flame is restricted in the miniature channel, and makes the flame front acting like a piston that compress the fresh mixture and generate induced flow ahead of flame. As the flame propagates into the induced flow under the influence of wall viscous effect, the flame front is elongated and the propagation velocity increases with enhancing flame area. The small size of the channel also lead to choking of the induced flow such that a leading shock is formed at 43.32 μs in Fig. 4. The propagation speed of the leading shock is ~550 m/s. Early formation of the leading shock retards the initial acceleration of the flame due to hydraulic resistance [18], and the flame propagates at a quasi-steady velocity of ~350 m/s after the leading shock appears.

Since the shock front is propagating faster than the reaction front, distance between the leading shock and the reaction front increases during the quasi-steady stage, which allows the boundary layers

behind the shock to grow [19,20]. The boundary layer in the unburned gas ahead of the flame lead to further stretching and distortion of the flame front, and the increasing flame area triggers the 2nd FA stage. The pre-compression and pre-heating effects of the leading shock can also be instrumental for the re-acceleration, but the arrival time difference between the leading shock and the reaction fronts is far shorter than the induction time required for immediate igniting the stoichiometric ethylene/oxygen mixture through the leading shock. Compression waves between the stretched flame front and side walls emerges during the 2nd FA stage (see frame 74.82 μs in Fig. 4). These compression waves right in front of the flame not only result in more intense pre-compression and pre-heating but also further perturb the flame front to enlarge the flame area. The overall outcome is a positive cycle for enhancing burning rate; the reaction front therefore continues to accelerate. The distance between the fronts reaches its maximum, which is ~ 8 mm, near the end of the 2nd FA stage.

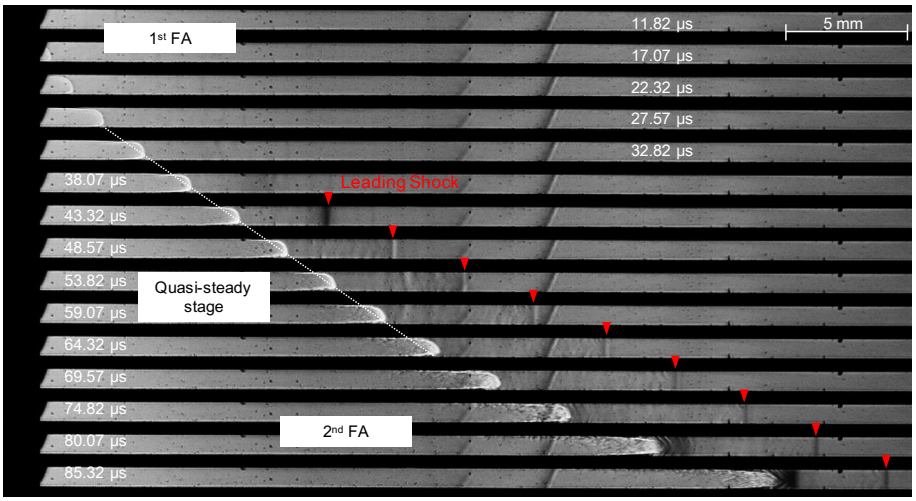

Figure 4. Schlieren images of 1st FA, quasi-steady stages and the transition to 2nd FA stage.

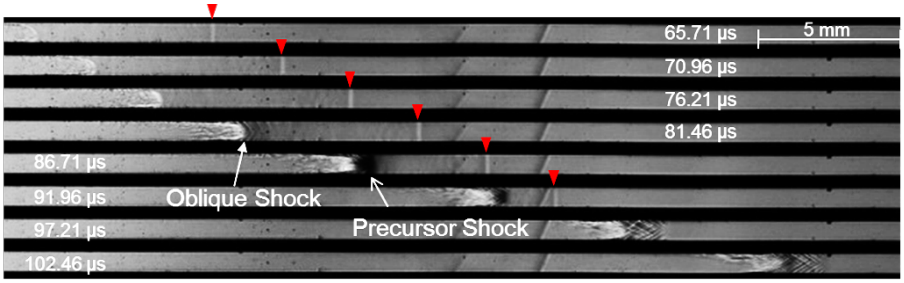

Figure 5. 2nd FA and transition to 3rd FA stage schlieren images

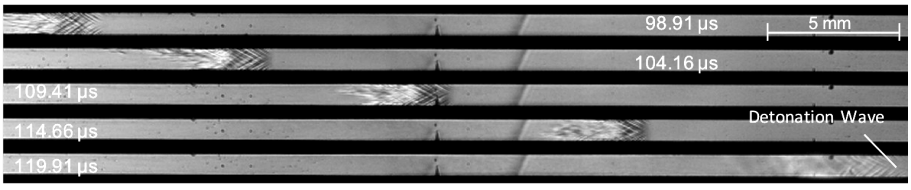

Figure 6. 3rd FA stage and final transition to detonation

The compression waves between the flame front and the walls quickly strengthen into oblique shocks, and coalesce to a precursor shock as shown in Fig. 5. The appearance of the precursor shock right ahead of flame indicates the inception of the 3rd FA stage, in which the reaction front velocity increases almost linearly with time. The size of the reaction zone becomes larger and brighter in the 3rd FA stage, and the front structure also looks different. The precursor shock develops into a staggered series of oblique shocks in front of the reaction wave after 97.21 μs in Fig. 5. Induction time of the unburned mixture could be largely shortened by pre-compression and pre-heating of the oblique shocks. The composite front will continue to accelerate for 20 - 25 μs until the propagation velocity reaches ~ 1500 m/s. Finally, local explosion occurs and drives the reaction wave into detonative state at 119.91 μs in Fig. 6.

5 Conclusion

Complete evolvements of reaction and shock waves of stoichiometric ethylene and oxygen mixture in a 1 mm * 1 mm channel were successfully resolved using a high-speed schlieren system. Four reaction propagation stages named, in the order of appearance, 1st FA, quasi-steady, 2nd FA and 3rd FA, were identified prior to the velocity surge associated with detonation transition. A leading shock developed ahead of the flame during the transition from 1st FA to the quasi-steady stage. The flame was stretched and oblique shocks were formed between the flame front and the walls in the 2nd FA stage. A precursor shock right in front of the flame which later developed into a staggered series of oblique shocks structure was the typical schlieren pattern observed during the 3rd FA stage. Growth rate of the reaction front velocity was found to follow power law in the 2nd FA stage, while the slope was linear in the 3rd FA phase. Local explosion drove the reaction front into detonation state at the end of the 3rd FA stage, when the reaction propagation velocity reached ~ 1500 m/s.

References

[1] D.M. Valiev, V. Akkerman, M. Kuznetsov, L.E. Eriksson, C.K. Law, V. Bychkov (2013), Combust. Flame 160(1): 97–111.
[2] V. N. Kurdyumov and M. Matalon (2013), Proc. Combust. Inst. 34: 865–872.
[3] V. Akkerman, C.K. Law, V. Bychkov, L.E. Eriksson (2010), Phys. Fluids 22: 053606.
[4] M.-H. Wu, P. Burke, S.F. Son, R.A Yetter (2007), Proc. Combust. Inst. 31: 2429-2439.
[5] M.-H. Wu, W.-C. Kuo (2013), Proc. Combust. Inst. 34: 2017–2024.
[6] M.-H. Wu, C.-Y. Wang (2011), Proc. Combust. Inst. 33: 2287.
[7] M.-H. Wu and W.-C. Kuo (2012), Combust. Flame 159: 3414-3422.
[8] L. Kagan, G. Sivashinsky (2010), Flow, Turbul. Combust. 84: 423–437.
[9] Y. Gao, H.D. Ng, J.H.S. Lee (2015), Combust. Flame, 162(6): 2405-2413.
[10] M.H. Wu and T.H. Lu (2012), J.. Micromech. Microeng. 22: 105040.
[11] P. Urtiew, A.K. Oppenheim (1966), Proc Roy Soc Lond Ser. A 295: 13-28.
[12] Y.B. Zeldovich, V.B. Librovitch, G.M. Makhviladze, G.I. Sivashinsky (1970), Astonaut. Acta: 15313–321.
[13] E.S. Oran, V.N. Gamezo (2006), Combustion and Flame. 186: 1758-1773
[14] J.H. Lee (1980), I.O. Moen, Prog. Energy Combust. Sci. 6: 350-389.
[15] J. E. Shepherd, J. H. S. Lee, Major Research Topics in Combustion, Springer-Verlag, Hampton, 1992.
[16] G. Ciccarelli, S. Dorofeev (2008), Prog. Energy Combust. Sci. 34: 499.
[17] V. Bychkov, V. Akkerman V, G. Fru, A. Petchenko, L.E. Eriksson (2007), Combust. Flame 150: 263-276
[18] D.M. Valiev, V. Bychkov, V. Akkerman, L.E. Eriksson, C.K. Law (2013), Phys. Fluids 25: 096101.
[19] M. Kuznetsov, V. Alekseev, I. Matsukov, S. Dorofeev (2005),. Shock Waves 14: 205-15.
[20] E. Dzieminska, A.K. Hayashi AK. (2013), Int J Hydrogen Energy 38: 4185-4193.